Study of lattice dynamics via extended x-ray absorption fine structure

2001 J. Phys.: Condens. Matter 13 7859

(http://iopscience.iop.org/0953-8984/13/34/324)

INSTITUTE OF PHYSICS PUBLISHING JOURNAL OF PHYSICS: CONDENSED MATTER

J. Phys.: Condens. Matter **13** (2001) 7859–7872 PII: S0953-8984(01)25537-4

Study of lattice dynamics via extended x-ray absorption fine structure

P Fornasini

Istituto Nazionale per la Fisica della Materia and Dipartimento di Fisica, Università di Trento, I-38050 Povo (Trento), Italy

E-mail: fornasin@science.unitn.it

Received 6 June 2001
Published 9 August 2001
Online at stacks.iop.org/JPhysCM/13/7859

Abstract

EXAFS (extended x-ray absorption fine structure), besides being a powerful structural probe, can also give original information on local dynamics in solids. EXAFS is peculiarly sensitive to the correlation of vibrational motion, both parallel and perpendicular to the bond direction, and to anharmonicity. This paper contains an introduction to the effects of thermal disorder on EXAFS of crystals and to the data analysis based on the cumulant expansion. Cumulants are easily connected to average local vibrational properties. Recently obtained experimental results concerning the mean square relative displacement and the thermal expansion in crystals confirm the potentialities of EXAFS as a dynamical probe.

1. Introduction

The acronym EXAFS (extended x-ray absorption fine structure) refers to the oscillations of the x-ray absorption coefficient of molecular and condensed systems, which are observed on the high-energy side of an absorption edge [1, 2]. The origin of EXAFS is easily understood on phenomenological grounds. When an x-ray photon of high enough energy is absorbed by an atom, an electron is ejected from a core orbital and leaves the atom, but has a finite probability of being back-scattered by other neighbouring atoms. The absorption coefficient depends, to first order, on the dipole matrix element connecting the initial core state ψ_i and the photoelectron final state ψ_f, which in turn is a superposition of the outgoing spherical wave and the incoming back-scattered wave. The phase relationship between outgoing and incoming waves depends on the product kR of photoelectron momentum and interatomic distance. The variation of the phase relationship as a function of photon energy modulates the final-state amplitude at the core site and thence the absorption coefficient. Consequently, the frequency of EXAFS oscillations depends on interatomic distances, and their amplitude is proportional to the number of neighbouring atoms.

0953-8984/01/347859+14$30.00

Two main peculiarities characterize EXAFS: (a) the selectivity as regards the atomic species, which is achieved by tuning the x-ray energy to the corresponding absorption edge; (b) the insensitivity to long-range order, due to the short photoelectron mean free path. This last property implies similarity between EXAFS spectra of amorphous and crystalline materials. In the last three decades EXAFS has developed into a powerful probe of local structure around selected atomic species in complex and disordered systems, like amorphous semiconductors, multicomponent oxide glasses, inorganic and biological catalysts, and randomly distributed solid solutions [3, 4]. The structural information extracted from EXAFS concerns the interatomic distance and coordination number of a few coordination shells of the absorbing atom.

This basic structural information is influenced by thermal disorder, whose main effect is a reduction of the amplitude of the EXAFS oscillations, analogous to the reduction of the peak intensity in diffraction patterns of crystals. A more subtle effect concerns the phase of the EXAFS oscillations. The study of these effects allows one to obtain original information not only on the thermodynamical properties of structurally disordered solids, but also on the lattice dynamics of crystals.

The peculiarities of EXAFS for dynamical studies are mainly based on the following properties:

(a) owing to the high values of transferred momentum, EXAFS is generally more sensitive than x-ray diffraction to disorder and in particular to anharmonicity;

(b) EXAFS is sensitive to the mean square *relative* displacement $\langle \Delta u^2 \rangle$ of absorber and back-scatterer atoms, which depends not only on the separate vibrational motion of the two atoms, but also on their correlation.

The potentialities of EXAFS as a dynamical probe [5, 6] as well as the sensitivity to anharmonicity [7] were pointed out quite early. However, after a few pioneering experimental works, only occasional use has been made of EXAFS to study vibrational properties in solids. Extended compilations of experimental results can be found in recent review papers [8, 9]. The development of theoretical work [10–12] and the increased accuracy of experimental results [13] are now renewing interest in the subject: on the one hand, the careful treatment of anharmonicity is giving new insights into the correlation and into local thermal expansion; on the other, there is a growing awareness that the accuracy of structural parameters, like interatomic distances, depends on an appropriate treatment of dynamical phenomena.

This paper is intended as an introduction to the use of EXAFS for dynamical studies. Self-consistency and comprehensibility for non-specialists are sought rather than generality and completeness. To this end, only crystalline systems are considered, the data analysis is restricted to within the single-scattering approximation, and a phenomenological approach is maintained throughout the paper. References to more exhaustive treatments are given anyway for interested readers.

In section 2 the basic theory of EXAFS is outlined and the procedure of data analysis based on the cumulant expansion, particularly suited for dynamical studies, is depicted. In section 3 the general relations connecting EXAFS parameters to atomic thermal displacements in the harmonic approximation are given, and a phenomenological approach to anharmonicity is attempted. Section 4 is specifically dedicated to the mean square relative displacement (MSRD): the sensitivity to correlation and the effects of anharmonicity are illustrated by suitable examples. In section 5 some recent advances in the study of thermal expansion are presented. Section 6 is dedicated to conclusions.

2. The EXAFS spectroscopy

The EXAFS function (figure 1) is defined as

$$\chi(k) = (\mu - \mu_0)/\mu_0 \tag{1}$$

where μ is the measured oscillating absorption coefficient and μ_0 the smooth absorption coefficient of an isolated atom. The EXAFS signal is conveniently expressed in (1) as a function of the photoelectron wavenumber k:

$$k = \sqrt{(2m_e/\hbar^2)(\hbar\omega - E_b)} \tag{2}$$

where $\hbar\omega$ is the x-ray photon energy and E_b the binding energy of the core electron.

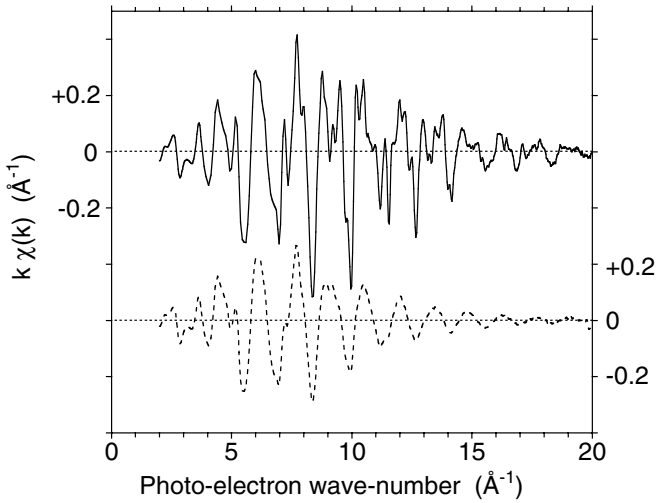

Figure 1. The EXAFS $k\chi(k)$ of germanium at 10 K (continuous line) and 300 K (dashed line). The signal at 10 K is the superposition of the contributions from several coordination shells. When temperature increases, EXAFS is damped; the damping is stronger for the outer shells, and the signal appears less structured.

2.1. The basic mechanism of EXAFS

The quantitative interpretation of EXAFS relies on the quantum picture of two stationary photoelectron spherical waves, the outgoing one and the back-scattered incoming one, whose interference affects the x-ray absorption probability. Let us outline here just the main steps leading to a parametrized formula for the EXAFS function (1) (more exhaustive treatments can be found in [2–4, 14], and references therein).

The x-ray absorption coefficient depends on the probabilities of transition, W_{fi}, from the initial state i to all the possible final states f:

$$\mu(\omega) \propto \sum_f W_{fi}. \tag{3}$$

The calculation of the transition probabilities is done within the framework of the time-dependent perturbation theory, leading, to first order, to the golden rule

$$W_{fi} = (2\pi/\hbar)\left|\langle\Psi_i|\hat{H}_I|\Psi_f\rangle\right|^2 \rho(E_f) \tag{4}$$

where $|\Psi_i\rangle$ and $|\Psi_f\rangle$ are the initial and final states of the absorber atom, respectively, $\rho(E_f)$ is the density of final states, and $\hat{H}_I$ is the interaction Hamiltonian.

By focusing on a transition involving only one selected core electron and truncating the interaction Hamiltonian expansion to the electric dipole term, the absorption coefficient can be expressed as

$$\mu(\omega) \propto \left|\langle\psi_i|\hat{\boldsymbol{\eta}}\cdot\boldsymbol{r}|\psi_f\rangle\right|^2 S_0^2\rho(\epsilon_f) \tag{5}$$

where now $|\psi_i\rangle$ and $|\psi_f\rangle$ are one-electron states, and $\rho(\epsilon_f)$ is the corresponding density of final states; $\boldsymbol{r}$ is the electron position and $\hat{\boldsymbol{\eta}}$ the electric field polarization unit vector. The many-body excitations competitive with the one-electron transition are taken into account by the unitless term S_0^2 (typically 0.6 to 0.9).

The initial state $|\psi_i\rangle$ in (5) is a localized core-electron wavefunction. If the atom is isolated, the final state is an outgoing spherical wave, $|\psi_f^0\rangle$, and equation (5) gives the atomic absorption coefficient μ_0. For an atom embedded in a molecule or a condensed system, the final state is instead the superposition of the outgoing spherical wave and the weak incoming waves due to the scattering from neighbouring atoms: $|\psi_f^0 + \delta\psi_f\rangle$. If one considers only photoelectrons of relatively high energy (typically higher than 30 to 50 eV), the final state can be calculated by the scattering theory in the plane-wave approximation. Combining then μ and μ_0 in (1), one gets the final formula

$$\chi(k) = (S_0^2/k)\sum_s N_s \,\mathrm{Im}\left\{f_s(k)\exp(2\mathrm{i}\delta_1)\frac{\exp(-2R_s/\lambda)}{R_s^2}\exp(2\mathrm{i}kR_s)\right\}. \tag{6}$$

In (6) the summation is over the few coordination shells of the absorber atom which give a significant contribution to EXAFS; R_s and N_s are the interatomic distance and coordination number, respectively, of the sth shell. The basic interference term is $\exp(2\mathrm{i}kR_s)$. λ is the photoelectron mean free path (typically 6 to 10 Å), $f_s(k)$ is the complex back-scattering amplitude, and δ_1 is the phase-shift due to the potential of the absorber atom.

The EXAFS signal can extend to values of exchanged momentum $2k$ as high as 30 or even 40 Å^{-1}, depending on sample composition and temperature. Conversely, the simple interpretation depicted in (6) cannot generally be utilized for $2k$ less than about 6 Å^{-1}. Equation (6) is based on the hypothesis that the photoelectron undergoes only one scattering event (single-scattering approximation); when multiple-scattering events cannot be neglected, more elaborate interpretation schemes should be used [10, 12]. In some cases also the plane-wave description of scattering fails, and a dependence on distance should be considered for the back-scattering amplitude $f_s(k, R)$. In the following we will consider only cases for which the single-scattering and plane-wave approximations are appropriate.

2.2. Effects of thermal disorder on EXAFS

Equation (6) refers to the unrealistic case of atoms frozen at their equilibrium positions. Thermal disorder spreads atomic positions into three-dimensional distributions. The photoelectron time of flight ($\sim 10^{-16}$ s) is much shorter than the period of atomic vibrations ($\sim 10^{-13}$ s), so an EXAFS spectrum samples a one-dimensional distribution of instantaneous interatomic distances r. For each coordination shell, equation (6) transforms into [15]

$$\chi_s(k,T) = (S_0^2/k)N_s \,\mathrm{Im}\left[f_s(k)\exp(2\mathrm{i}\delta_1)\int_0^\infty \rho(r,T)\frac{\exp(-2r/\lambda)}{r^2}\exp(2\mathrm{i}kr)\,\mathrm{d}r\right]. \tag{7}$$

The function $\rho(r, T)$ represents the pair distribution of absorber–back-scatterer distances, averaged over the coordination shell. It is referred to as the *real distribution*, while the

r-dependent factors within (7) are globally referred to as the *effective distribution*:

$$P(r, \lambda, T) = \rho(r, T) \exp(-2r/\lambda)/r^2. \tag{8}$$

The distribution $\rho(r, T)$ contains all structural and dynamical information in principle available from EXAFS. The inversion of equation (7) to recover $\rho(r, T)$ from $\chi(k, T)$ cannot be done exactly, mainly because of the limited k-range of experimental spectra. Various approximate solutions have been proposed for this problem; the one based on the *cumulant expansion* is particularly appropriate for dynamical studies [15–17]. Basically, the structural part of the EXAFS formula (7) can be expanded as a MacLaurin series in the wavenumber k:

$$\ln \int_0^\infty P(r, \lambda, T) \exp(2ikr)\, dr = \sum_{n=0}^{\infty} (2ik)^n C_n(T)/n! \tag{9}$$

where $C_n(T)$ are the *cumulants* of the effective distribution $P(r, \lambda, T)$. Taking into account (9) and readjusting $f_s(k) \exp(2i\delta_1) = |f_s(k)| \exp(i\phi)$, equation (7) is written in the more explicit real form

$$\chi_s(k, T) = (S_0^2/k) N_s |f_s(k)| \exp(C_0 - 2k^2 C_2 + 2k^4 C_4/3 - \cdots) \times \sin[2kC_1 - 4k^3 C_3/3 + \cdots + \phi(k)]. \tag{10}$$

Odd and even cumulants determine the phase and amplitude of the EXAFS signal, respectively. The cumulants have a simple physical interpretation. C_0 depends on the normalization of the effective distribution: $\exp(C_0) \simeq \exp(-2C_1/\lambda)/C_1^2$. C_1 and C_2 are the mean value and the variance of the distribution, respectively. Higher-order cumulants are zero for Gaussian distributions. C_3 and higher-order odd cumulants depend on the asymmetry of the distribution. C_4 and higher-order even cumulants describe symmetric deviations from the Gaussian shape.

For weak disorder only the first cumulants (C_0, C_1, and C_2) are significant, the effective distribution can be considered Gaussian, and equation (10) reduces to the frequently used *standard formula* for EXAFS:

$$\chi_s(k, T) = (S_0^2/k) N_s |f_s(k)| \frac{\exp(-2C_1/\lambda)}{C_1^2} \exp(-2k^2 C_2) \sin[2kC_1 + \phi(k)]. \tag{11}$$

Here thermal disorder only broadens the Gaussian distribution, causing an exponential damping of the EXAFS signal, which is measured by the *EXAFS Debye–Waller factor* $\exp(-2k^2 C_2)$.

The standard formula (11) can safely be used only for low-temperature spectra, when anharmonic contributions are negligible. When the Debye temperature is approached, anharmonic effects cannot in any case be neglected: the Gaussian approximation is no longer valid, higher-order cumulants become important, and equation (10) should be used: thermal disorder influences not only the variance of the distribution, but also its overall shape; odd cumulants, related to asymmetry, modify also the phase of the EXAFS signal. When the temperature grows further, a larger number of cumulants become significant, and eventually the convergence interval of the cumulant series becomes shorter than the EXAFS range, so not even equation (10) can be used safely [17]. Here we will consider only cases for which equation (10) is applicable.

Equation (10) expresses EXAFS as a function of the cumulants $C_i(T)$ of the *effective* distribution $P(r, \lambda, T)$, while one is interested in the corresponding cumulants $C_i^*(T)$ of the *real* distribution $\rho(r, T)$.

The first cumulant (mean value) of the effective distribution is systematically smaller than the first cumulant of the real distribution, as a consequence of the spherical nature of the photoelectron wave and its limited mean free path [15]:

$$C_1 = C_1^* - (2C_2^*/C_1^*)(1 + C_1^*/\lambda). \tag{12}$$

The difference between the first cumulants cannot be neglected in highly accurate works (see section 5). The difference between the second- and higher-order cumulants of the two distributions [18] can however be neglected for not-too-disordered systems.

2.3. Measurement and data analysis

The ideal x-ray source for EXAFS is synchrotron radiation, owing to the intense continuous spectrum and the intrinsic vertical collimation [19]. In direct transmission measurements the x-ray energy is tuned by Bragg reflection from a pair of parallel crystals, and the beam intensity is measured in front of and beyond the sample by two detectors, typically ionization chambers. The sample is generally powdered, and its thickness is of the order of 10 μm. Other more sophisticated detection schemes are used for particular cases (diluted samples, surface studies, etc) [3]. For dynamical studies, measurements are made at different temperatures, which is relatively simple and fast, since the sample is fixed and can be easily cooled or heated.

The first step of the data analysis consists in the extraction of the EXAFS function (1) from the experimental absorption coefficient (figure 1). The contributions of the different coordination shells are then singled out by Fourier filtering and separately analysed (figure 2). If the 'physical' factors S_0^2, $|f_s(k)|$, and $\phi(k)$ are known from theoretical calculations or from suitable reference compounds, by fitting equation (10) to the experimental spectra one gets the 'structural' parameters $C_i(T)$. In dynamical studies one often extracts the physical factors from the lowest-temperature spectrum, taken as reference. In this way one gets the temperature dependence $\Delta C_i(T) = C_i(T) - C_i(T_0)$ of cumulants relative to the low-temperature spectrum (figure 3). To obtain absolute values $C_i(T)$, when required, one fits the temperature dependence $\Delta C_i(T)$ using suitable models (see below). The alternative procedure of using calculated physical parameters directly gives absolute values $C_i(T)$, whose accuracy however depends critically on the soundness of assumptions and approximations of theoretical calculations.

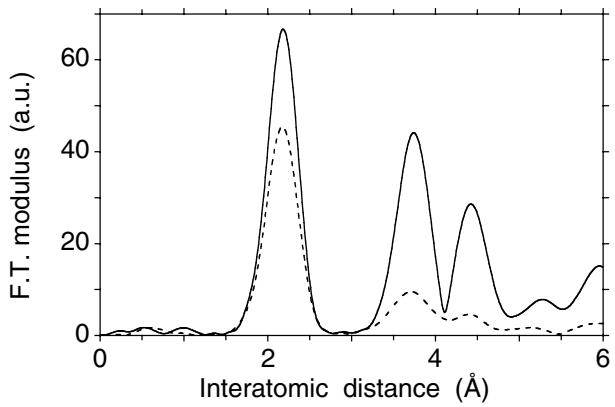

Figure 2. Fourier transforms of the EXAFS signal of germanium at 10 K (continuous line) and 300 K (dashed line). The peaks correspond to the contributions of different coordination shells (the peak positions differ from the real distances as a consequence of the term $\phi(k)$ in the EXAFS phase). The thermal damping is stronger for the outer shells.

3. EXAFS and dynamical properties

We want now to see how the EXAFS parameters, say the cumulants $C_i(T)$ and $C_i^*(T)$ of the effective and real distributions, are connected to vibrational properties of crystals. The

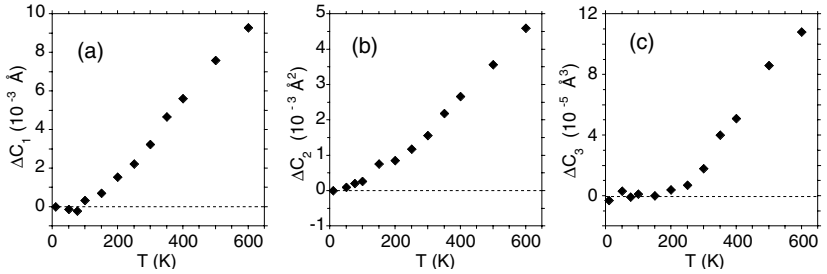

Figure 3. Temperature dependences of the first three cumulants C_i of the first coordination shell of germanium, determined from EXAFS analysis taking the 10 K spectrum as reference [13]. The usual Einstein-like behaviour of C_2 is evident (b). Low-temperature quantum deviations from the classical behaviours, equations (23)–(25), are noticeable also for C_1 (a) and C_3 (c).

cumulants describe average properties of the distributions of distances:

$$C_1^*(T) = \langle r \rangle \qquad C_2^*(T) = \langle (r - \langle r \rangle)^2 \rangle \qquad C_3^*(T) = \langle (r - \langle r \rangle)^3 \rangle. \tag{13}$$

The distance r in turn depends on the instantaneous atomic thermal displacements. Let us consider the absorber atom and one of its neighbours, labelled 0 and j, respectively. Let $\boldsymbol{R}$ be the equilibrium distance, $\boldsymbol{r}$ the instantaneous distance, and $\Delta\boldsymbol{u} = \boldsymbol{u}_j - \boldsymbol{u}_0$ the instantaneous relative displacement:

$$\boldsymbol{r} = \boldsymbol{R} + \Delta\boldsymbol{u}. \tag{14}$$

In the following we will consider the projections of the relative displacement $\Delta\boldsymbol{u}$ parallel and perpendicular to the interatomic bond, defined by

$$\Delta u_\parallel = \hat{\boldsymbol{R}} \cdot \Delta\boldsymbol{u} \qquad (\Delta u_\perp)^2 = (\Delta u)^2 - (\Delta u_\parallel)^2. \tag{15}$$

From (14) and (15) it is straightforward to derive the approximate expression for the scalar distance r:

$$r \simeq R + \Delta u_\parallel + (\Delta u_\perp)^2/2R - [\Delta u_\parallel (\Delta u_\perp)^2]/2R^2. \tag{16}$$

3.1. Harmonic approximation

In the harmonic approximation for the crystal potential, the averages (13) are connected to the atomic displacements by simple first-order relations. Starting from equation (16) it is easy to show that

$$C_1^* \simeq R + \langle (\Delta u_\perp)^2 \rangle / 2R \tag{17}$$

$$C_2^* \simeq \left\langle (\Delta u_\parallel)^2 \right\rangle. \tag{18}$$

The third cumulant C_3^* is generally negligible for a harmonic crystal potential, although the distribution $\rho(r)$ is not strictly symmetrical. As a consequence, the standard formula (11) can be used.

According to equation (18), the second cumulant, which measures the exponential thermal damping of the EXAFS signal, directly gives the quantity $\langle (\Delta u_\parallel)^2 \rangle$, generally referred to as the *mean square relative displacement* (MSRD) and indicated by σ^2 [5]. We will consider the MSRD further in section 4.

Let us now turn to equation (17). The mean value C_1^* of the real distribution is larger than the equilibrium distance R, owing to the relative thermal motion perpendicular to the bond direction [18, 20]. Since $\langle (\Delta u_\perp)^2 \rangle$ grows with temperature, it generates an apparent thermal

expansion also for an ideally harmonic crystal. By comparing equations (12) and (17), one can see that the apparent expansion is of the same order as the difference between C_1 and C_1^*, but of opposite sign, so in many cases C_1 can be confused with R within the experimental uncertainties. However, when the experimental accuracy is high enough, the effects of $\langle(\Delta u_\parallel)^2\rangle$ in (12) and $\langle(\Delta u_\perp)^2\rangle$ in (17) should be separately taken into account (figure 5—see later). The MSRD $\langle(\Delta u_\parallel)^2\rangle$ can be obtained from experimental EXAFS spectra, through equation (18). The quantity $\langle(\Delta u_\perp)^2\rangle$ has instead to be calculated independently, since its connection with $\langle(\Delta u_\parallel)^2\rangle$ depends on the particular crystal structure [21]. As a consequence, an accurate determination of the interatomic distance R and of the thermal expansion cannot be made solely from an EXAFS experiment. Conversely, the comparison of the EXAFS C_1^* with R (known from other techniques) allows one to obtain the quantity $\langle(\Delta u_\perp)^2\rangle$. We will come back to this topic in section 5.

In the harmonic approximation the instantaneous displacement of the jth atom within the ℓth unit cell can be expressed as [22]

$$\boldsymbol{u}_{\ell j}(t) = (\mathcal{N} m_j)^{-1/2} \sum_{\boldsymbol{q},\lambda} Q(\boldsymbol{q},\lambda,t)\boldsymbol{w}_j(\boldsymbol{q},\lambda)\exp(\mathrm{i}\boldsymbol{q}\cdot\boldsymbol{r}_{\ell j}) \tag{19}$$

where $\mathcal{N}$ is the number of unit cells and m_j and $\boldsymbol{r}_{\ell j}$ are the mass and the vector position of the atom, respectively. $Q(\boldsymbol{q},\lambda,t)$ is the (complex) normal coordinate of mode $(\boldsymbol{q},\lambda)$ and $\boldsymbol{w}_j(\boldsymbol{q},\lambda)$ are normalized eigenvectors of the dynamical matrix

$$\mathcal{D}_{j\alpha,j'\beta}(\boldsymbol{q}) = (m_j m_{j'})^{1/2} \sum_{\ell'} \Phi_{\ell j\alpha,\ell' j'\beta} \exp\left[-\mathrm{i}\boldsymbol{q}\cdot(\boldsymbol{r}_{\ell j} - \boldsymbol{r}_{\ell' j'})\right] \tag{20}$$

where the Φ are the force constants and α, β label the x-, y-, z-coordinates.

Once the dynamical matrix and its eigenvalues and eigenvectors have been calculated, the quantities $\langle(\Delta u_\parallel)^2\rangle$ and $\langle(\Delta u_\perp)^2\rangle$ can be evaluated and compared with the values obtained from the EXAFS.

3.2. Anharmonicity

The sensitivity of EXAFS to anharmonicity depends on the relatively high values of the exchanged momentum $2k$: the weight of the cumulant of order n in (10) grows with the nth power of k. After the first pioneering works on CuBr [23] and AgI [17], it became clear that anharmonicity could not be neglected even for systems like germanium or GaAs [24, 25]. Several theoretical schemes of different degrees of complexity and generality have been developed for the interpretation of anharmonicity effects in EXAFS [11, 23, 26, 27]. Here we will rely on a semi-classical approach which is frequently used in phenomenological analyses.

The distribution $\rho(r)$ of interatomic distances is connected to an *effective pair potential* V_e [28]. In the classical approximation, for sufficiently high temperatures,

$$\rho(r,T) = \exp[-\beta V_e(r)]\left\{\int \exp[-\beta V_e(r)]\,\mathrm{d}r\right\}^{-1} \tag{21}$$

where $\beta = 1/k_B T$. The potential V_e can be expanded as

$$V_e(u) = au^2/2 + bu^3 + cu^4 + \cdots \tag{22}$$

where u is the variation of interatomic distance with respect to the potential minimum.

In the classical approximation the first four cumulants of the distribution $\rho(r,T)$ can be related to the force constants $a, b, c, \ldots$ of the effective potential V_e by [23, 29]

$$\delta C_1^*(T) = -(3b/a^2)k_B T + \cdots \tag{23}$$

$$C_2^*(T) = (k_B T/a) + (k_B T/a)^2\left[(6b/a)^2 - (12c/a)\right] + \cdots \tag{24}$$

$$C_3^*(T) = -(k_B T/a)^2(6b/a) + \cdots \tag{25}$$

$$C_4^*(T) = (k_B T/a)^3\left[(108b^2/a^2) - (24c/a)\right] + \cdots . \tag{26}$$

The linear growth of δC_1^* with temperature in (23) depends on the potential asymmetry, and is reproduced, to first order, also by the ratio $C_3^*/2C_2^*$. Always to first order and in the classical approximation, C_2^* grows linearly with T (harmonic approximation), while C_3^* and C_4^* go like T^2 and T^3, respectively. Equation (24) shows also the second-order anharmonic correction to C_2^*.

Low-temperature quantum deviations of C_2^* from the classical behaviour (24) are never negligible (figure 3(b)), and the linear dependence on temperature has to be replaced by the Bose–Einstein population factor (see equation (29) below). Quantum corrections to higher-order cumulants have also been calculated [11, 26], and can sometimes be non-negligible (figure 3(c)) [13]. Apart from the classical approximation, equations (23)–(26) rely also on the hypothesis that the potential V_e is independent of temperature, both in shape and in position. This hypothesis is not necessarily fulfilled: the effective one-dimensional potential V_e depends on the statistically averaged behaviour of all the atoms in the crystal, and can be temperature dependent.

4. Mean square relative displacement

Let us now focus our attention on the mean square relative displacement (MSRD). Starting from equation (15), the MSRD of the absorber–back-scatterer pair of atoms can be expressed as

$$\langle(\Delta u_\parallel)^2\rangle = \langle(\hat{\boldsymbol{R}}\cdot\Delta\boldsymbol{u})^2\rangle = \langle(\hat{\boldsymbol{R}}\cdot\boldsymbol{u}_j)^2\rangle + \langle(\hat{\boldsymbol{R}}\cdot\boldsymbol{u}_0)^2\rangle - 2\langle(\hat{\boldsymbol{R}}\cdot\boldsymbol{u}_j)(\hat{\boldsymbol{R}}\cdot\boldsymbol{u}_0)\rangle. \tag{27}$$

The first two terms on the right-hand side represent the mean square displacements (MSDs) of absorber and back-scatterer atoms, respectively, while the last term is the displacement correlation function (DCF) [5].

4.1. MSRD in the harmonic approximation

Substituting in (27) the atomic displacements (19), one obtains

$$\langle(\Delta u_\parallel)^2\rangle = \frac{1}{\mathcal{N}\mu}\sum_{\boldsymbol{q},\lambda}\langle|Q(\boldsymbol{q},\lambda,t)|^2\rangle\left|\hat{\boldsymbol{R}}\cdot\left(\frac{\boldsymbol{w}_j(\boldsymbol{q},\lambda)\exp(\mathrm{i}\boldsymbol{q}\cdot\boldsymbol{R})}{(m_j/\mu)^{1/2}} - \frac{\boldsymbol{w}_0(\boldsymbol{q},\lambda)}{(m_0/\mu)^{1/2}}\right)\right|^2 \tag{28}$$

where m_0 and m_j are the masses of the absorber and back-scatterer atoms, respectively, μ is their reduced mass, and the temperature dependence is given by

$$\langle|Q(\boldsymbol{q},\lambda,t)|^2\rangle = [\hbar/2\omega(\boldsymbol{q},\lambda)]\coth[\hbar\omega(\boldsymbol{q},\lambda)/2k_B T]. \tag{29}$$

When the square of the binomial expression inside the modulus bars in equation (28) is calculated, the two direct terms correspond to the uncorrelated MSDs of absorber and back-scatterer atoms, the cross product to the DCF.

The sensitivity of EXAFS to correlation can be better appreciated by the comparison with diffraction [30]. If we consider only a single pair of atoms, the Debye–Waller factor of diffraction $\exp[-G^2\langle(\hat{\boldsymbol{G}}\cdot\Delta\boldsymbol{u})^2\rangle/2]$ has the same expression as the EXAFS Debye–Waller factor $\exp[-2k^2\langle(\hat{\boldsymbol{R}}\cdot\Delta\boldsymbol{u})^2\rangle]$. $\boldsymbol{G}$ is the scattering vector of diffraction; the corresponding scattering vector in EXAFS has magnitude $2k$, and is directed along the bond direction $\hat{\boldsymbol{R}}$. The significant difference between EXAFS and diffraction appears when the entire crystal is taken into account. The EXAFS of one coordination shell is the sum of the contributions of *a few atomic pairs*, while a diffraction pattern is a sum over *all the atomic pairs* within the crystal.

As a consequence of long-range averaging, in diffraction the effect of short-range correlations is dispersed into the thermal diffuse scattering, and the Debye–Waller factor monitors only the uncorrelated MSD. By subtracting from the EXAFS MSRD the sum of the MSDs of absorber and back-scatterer atoms, measured by means of diffraction, one gets the value of the correlation function DCF.

For monatomic Bravais crystals, where only acoustic modes are present, the correlation depends only on the phonon wavevectors through the dot product $\boldsymbol{q} \cdot \boldsymbol{R}$ in (28). In non-Bravais crystals the phase relationships between eigenvectors add a significant, if not predominant, contribution to correlation. The correlation effect is stronger between nearest neighbours, say for the first coordination shell. When going from the first to the outer coordination shells, the correlation progressively decreases, and the EXAFS MSRD increases and tends to the sum of the MSDs of absorber and back-scatterer atoms.

The calculation of the MSRD (28) requires the knowledge of eigenvalues and eigenvectors of the dynamical matrix. Different dynamical models, though giving the same dispersion curves, can yield different eigenvectors [31]. The reproduction of the MSRD, in view of its peculiar sensitivity to correlation, represents an important independent test of dynamical calculations.

The effects of correlation are well illustrated by the case of β-AgI (figure 4, left). The thermal motion of silver ions, measured by means of diffraction, is more intense than that of iodine ions. As a consequence, the uncorrelated MSD of the I–Ag pair is larger than that of the I–I pair. Conversely, the MSRD of the first-shell I–Ag pair is smaller than that of the second-shell I–I pair, owing to a much stronger correlation effect. The dynamics of AgI is strongly characterized by the presence of very low-frequency optical modes. The temperature dependence of the MSRDs could be reproduced through equation (28) with eigenvectors calculated at the centre of the first Brillouin zone [32]. The difference in correlation between first and second shells is largely due to the different projections along the bond directions of the atomic displacements induced by the low-frequency optical modes. However, when the entire Brillouin zone was sampled, using eigenfrequencies and eigenvectors calculated through a valence shell model which satisfactorily reproduced the phonon dispersion

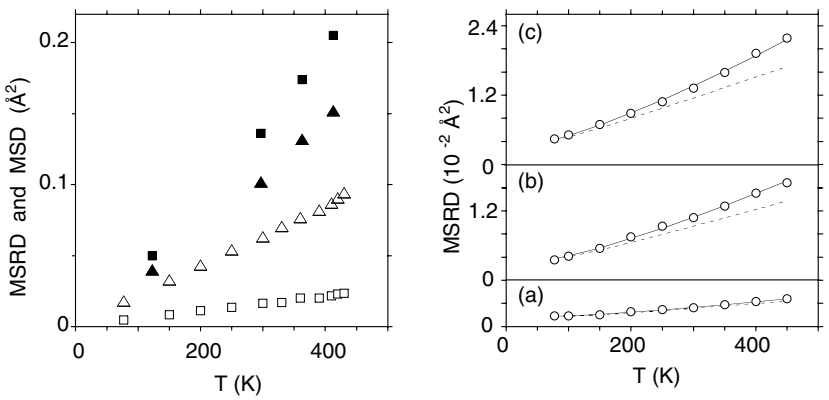

Figure 4. *Left panel:* correlation effects in the MSRD of β-AgI, taking iodine as the absorber atom. Open squares and triangles relate to the first-shell I–Ag and second-shell I–I MSRDs, respectively; full squares and triangles show the uncorrelated MSDs of the I–Ag and I–I pairs, respectively. *Right panel:* anharmonic effects on the MSRDs of the first three coordination shells in germanium (in order, (a), (b), and (c)). The circles show experimental values, the continuous line the best-fitting equation (31), the dashed line the corresponding harmonic contribution.

curves [33], the strong correlation effects experimentally found for the MSRD could not be reproduced at all.

As was pointed out in section 2, from the EXAFS analysis one often gets only relative values of the second cumulant, $\Delta C_2(T) = C_2(T) - C_2(T_0)$. Absolute values of the MSRD, such as those shown in figure 4, left, are generally recovered by fitting the temperature dependence of ΔC_2 to a phenomenological Einstein correlated model:

$$\sigma^2(\omega_E, T) = (\hbar/2\mu\omega_E)\coth(\hbar\omega_E/2kT) \tag{30}$$

depending on one parameter, the frequency ω_E [9]. In general the Einstein frequency ω_E does not correspond to defined peaks of the vibrational density of states. It can anyway be considered a measure of the effective bond-stretching force constant: $f = \mu\omega_E^2$. Its value can be utilized to estimate and compare the strength of different bonds.

4.2. Anharmonic contributions to the MSRD

Anharmonicity can affect the MSRD and modify its high-temperature behaviour, according to the second term in equation (24). An approximate expression for the MSRD, taking into account both low-temperature quantum effects and high-temperature anharmonicity, can be obtained from (24) by substituting an Einstein model (30) for the first linear term, with $a = \mu\omega_E^2$, and expressing the second term as a function of the cumulants C_3 and C_4:

$$C_2(T) = \sigma^2(\omega_E, T) - \frac{1}{2}\left(\frac{k_B T}{\mu\omega_E^2}\right)^2 C_3^2(T) + \frac{1}{2}\left(\frac{k_B T}{\mu\omega_E^2}\right) C_4(T). \tag{31}$$

If the third and fourth cumulants are known with good accuracy from experimental data, equation (31) contains only one free parameter ω_E and can be fitted to the slope of the experimental points $\Delta C_2(T)$, allowing the separation of the harmonic MSRD from the first-order anharmonic contribution.

The analysis based on equation (31) was applied to the MSRDs of the first three co-ordination shells of germanium [24]. The results are summarized in figure 4, right, where also the harmonic contribution $\sigma^2(\omega_E, T)$ is shown (dashed lines). The anharmonic expression (31) gave a better fit to the temperature dependence of the experimental values than a simple Einstein model (30), in particular for the outer shells. The soundness of this phenomenological procedure was confirmed by the comparison with *ab initio* calculations [34] made in the harmonic approximation and based on a perturbative approach to the density functional theory [35]. The theoretical values were in very good agreement both in slope and absolute value with the harmonic part of equation (31) [34]. The agreement would have been significantly worse, at least for the second and third shells, had only a harmonic model been fitted to experimental values.

5. Thermal expansion

The high sensitivity to anharmonicity suggests that EXAFS could be used to study local thermal expansion; this possibility, combined with the selectivity as regards atomic species, could be particularly useful for multicomponent non-crystalline systems or for low-concentration impurities. To achieve a better understanding of the strengths and limitations of EXAFS as a probe of thermal expansion, high accuracy measurements on crystals of known thermodynamical properties are being carried out.

According to the approximate classical equations (23)–(25), the thermal expansion could be measured equivalently by either δC_1^* or $C_3^*/2C_2^*$. This corresponds to saying that the

average position C_1^* of the distance distribution is completely determined by the asymmetry of the effective pair potential V_e. Actually, according to equation (17), C_1^* depends also on the apparent thermal expansion induced by vibrations normal to the bond. Measurements on several crystals, Ge [13], AgI [18], and CdSe [28], have shown that C_1^* always overestimates the real thermal expansion. The results for germanium are shown in figure 5.

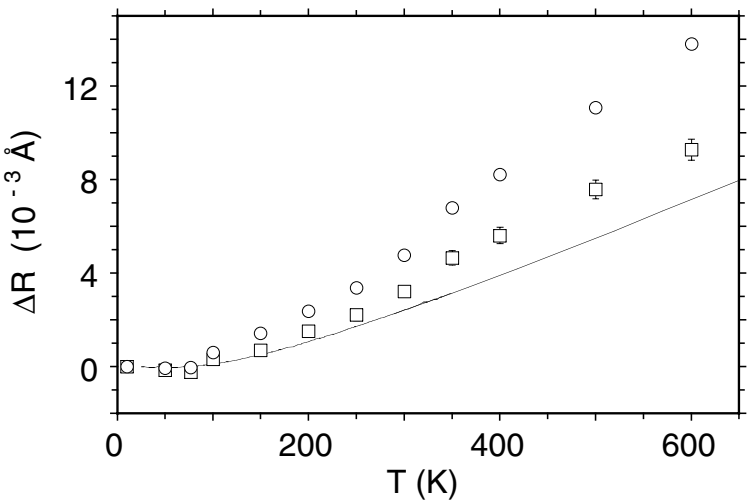

Figure 5. EXAFS and thermal expansion in germanium. The continuous line shows the thermal expansion expected for the nearest-neighbour distance [36]; squares and circles give the temperature variations of the first cumulants C_1 and C_1^* of the effective and real distributions, respectively.

In the case of germanium, the high quality of the experimental data has allowed for the first time the inversion of equation (17) to recover the quantity $\langle(\Delta u_\perp)^2\rangle$ as a function of temperature [13]. The reliability of the procedure is confirmed by the remarkable consistency between the ratio $\gamma = \langle(\Delta u_\perp)^2\rangle/\langle(\Delta u_\parallel)^2\rangle$ obtained from the EXAFS of germanium and the same ratio calculated for silicon on the basis of an adiabatic bond charge model [21].

Let us now consider the alternative possibility for measuring thermal expansion, say the ratio $C_3^*/2C_2^*$. In the case of germanium, if low-temperature quantum effects in C_3^* are taken into account according to the method suggested in [26], the ratio $C_3/2C_2$ reproduces well the real thermal expansion. However, in the case of CdSe and AgI the ratios $C_3/2C_2$ substantially overestimate the real thermal expansion [18, 28], which is actually very weak for CdSe and almost null for AgI. For these two crystals, then, the thermal expansion cannot be obtained either from the first or from the third cumulant.

The generally observed failure of the equivalence between δC_1^* and $C_3^*/2C_2^*$, postulated by equations (23)–(25), can be explained by assuming that the minimum position of the effective potential is temperature dependent. The growth of the mean value C_1^* with temperature is then a joint effect of the shift of the minimum position and the asymmetry of the potential. The results obtained for germanium suggest that the asymmetry of the *effective potential* reflects the anharmonicity of the *crystal potential*, so the third cumulant actually gives the thermal expansion. The thermal vibrations normal to the bond direction produce instead a positive shift of the minimum of the effective potential, which causes the apparent thermal expansion of the first cumulant, without affecting the shape of the potential. The situation is more complicated for CdSe and AgI. Here the minimum of the effective potential V_e exhibits a strong negative shift with temperature, probably connected with the anomalous thermal expansion

of these compounds. In the absence of an independent knowledge of the term $\langle(\Delta u_\perp)^2\rangle$, it is impossible to disentangle the three effects (downward shift of the potential minimum, thermal vibrations normal to the bond direction, anharmonicity) from the measurements of only two parameters (first and third cumulant).

6. Conclusions

EXAFS is particularly sensitive to the correlation of vibrational motion of neighbouring atoms, and can be used to test and compare the phase relationships between eigenvectors of different dynamical models. The quantity traditionally extracted from EXAFS is the MSRD parallel to the bond direction $\langle(\Delta u_\parallel)^2\rangle$. Recently more attention has been paid to the effects of anharmonicity: not only has a better agreement with theoretical calculations of $\langle(\Delta u_\parallel)^2\rangle$ been obtained by subtracting anharmonic contributions from experimental data, but also the possibility has been demonstrated of obtaining the correlation term $\langle(\Delta u_\perp)^2\rangle$ perpendicular to the bond direction.

Thermal expansion studies on crystals have shown that the effective EXAFS pair potential is temperature dependent. While for germanium this dependence is due only to the term $\langle(\Delta u_\perp)^2\rangle$, in other cases, like those of AgI and CdSe, the situation appears more complex and has not yet found an explanation. It is however reasonable to assume that the comparison between local properties sampled by EXAFS and average thermodynamic quantities could shed new light on peculiar phenomena, like local lattice distortions, opening new perspectives for EXAFS in crystals.

Once the subtle effects of correlation and anharmonicity are well understood for crystals, EXAFS could become an efficient probe not only of structure, but also of local dynamical properties of complex and amorphous systems.

Acknowledgments

The author is indebted to the many people who, at different times and at different levels, collaborated with him in studies of dynamics via EXAFS, in particular: G Dalba, R Grisenti, F Rocca, F Monti, S Mobilio, J Purans, A Kuzmin, D Diop, M Grazioli, R Gotter, D Pasqualini, A Sanson and S a Beccara.

References

[1] Sayers D E, Stern E A and Lytle F W 1971 *Phys. Rev. Lett.* **27** 1204
[2] Lee P A, Citrin P H, Eisenberger P and Kincaid B M 1981 *Rev. Mod. Phys.* **53** 769
[3] Hayes T M and Boyce J B 1982 *Solid State Physics* vol 37 (New York: Academic) p 173
[4] Koningsberger D C and Prins R (ed) 1988 *X-ray Absorption: Principles, Applications, Techniques of EXAFS, SEXAFS and XANES* (New York: Wiley)
[5] Beni G and Platzman P M 1976 *Phys. Rev.* B **34** 2293
[6] Sevillano E, Meuth H and Rehr J J 1979 *Phys. Rev.* B **20** 4908
[7] Eisenberger P and Brown G S 1979 *Solid State Commun.* **29** 481
[8] Tröger L, Yokoyama T, Arvanitis D, Lederer T, Tischer M and Baberschke K 1994 *Phys. Rev.* B **49** 888
[9] Dalba G and Fornasini P 1997 *J. Synchrotron Radiat.* **4** 143
[10] Benfatto M, Natoli C R and Filipponi A 1989 *Phys. Rev.* B **40** 9626
[11] Fujikawa T and Miyanaga T 1993 *J. Phys. Soc. Japan* **62** 4108
Miyanaga T and Fujikawa T 1998 *J. Phys. Soc. Japan* **67** 2930
[12] Poiarkova A V and Rehr J J 1999 *Phys. Rev.* B **59** 948
[13] Dalba G, Fornasini P, Grisenti R and Purans J 1999 *Phys. Rev. Lett.* **82** 4240
[14] Crozier E D 1997 *Nucl. Instrum. Methods* B **133** 134

[15] Crozier E D, Rehr J J and Ingalls R 1988 *X-ray Absorption: Principles, Applications, Techniques of EXAFS, SEXAFS and XANES* (New York: Wiley) p 373
[16] Bunker G 1983 *Nucl. Instrum. Methods* **207** 437
[17] Dalba G, Fornasini P and Rocca F 1993 *Phys. Rev.* B **47** 8502
[18] Dalba G, Fornasini P, Gotter R and Rocca F 1995 *Phys. Rev.* B **52** 149
[19] Koch E E (ed) 1980 *Handbook on Synchrotron Radiation* (New York: McGraw-Hill)
[20] Busing W R and Levy H A 1964 *Acta Crystallogr.* **17** 142
[21] Nielsen O H and Weber W 1980 *J. Phys. C: Solid State Phys.* **13** 2449
[22] Brüesch P 1982 *Phonons: Theory and Experiment* vol 1 (Berlin: Springer)
[23] Tranquada J M and Ingalls R 1983 *Phys. Rev.* B **28** 3520
[24] Dalba G, Fornasini P, Grazioli M and Rocca F 1995 *Phys. Rev.* B **52** 11 034
[25] Dalba G, Diop D, Fornasini P and Rocca F 1994 *J. Phys.: Condens. Matter* **6** 3599
[26] Frenkel A I and Rehr J J 1993 *Phys. Rev.* B **48** 585
[27] Yokoyama T, Kobayashi K, Ohta T and Ugawa A 1996 *Phys. Rev.* B **53** 6111
Yokoyama T, Yonamoto Y, Ohta T and Ugawa A 1996 *Phys. Rev.* B **54** 6921
[28] Dalba G, Fornasini P, Grisenti R, Pasqualini D, Diop D and Monti F 1998 *Phys. Rev.* B **58** 4793
[29] Stern E A, Livins P and Zhang Z 1991 *Phys. Rev.* B **43** 8850
[30] Willis B T M and Pryor A W 1975 *Thermal Vibrations in Crystallography* (Cambridge: Cambridge University Press)
[31] Cochran W 1971 *Acta Crystallogr.* A **27** 556
[32] Dalba G, Fornasini P, Rocca F and Mobilio S 1990 *Phys. Rev.* B **41** 9668
[33] Bührer W, Nicklow R M and Brüesch P 1978 *Phys. Rev.* B **17** 3362
[34] Strauch D, Pavone P, Nerb N, Karch K, Windl W, Dalba G and Fornasini P 1996 *Physica* B **219+220** 436
[35] Giannozzi P, de Gironcoli S, Pavone P and Baroni S 1991 *Phys. Rev.* B **43** 7231
[36] Touloukian Y S, Kirby R K, Taylor R E and Desai P D 1977 *Thermophysical Properties of Matter* vol 13 (New York: Plenum)